Oliveira, L. M. R. and Cardoso, A. J. M.: "A coupled electromagnetic transformer model for the analysis of winding inter-turn short-circuits", Record of the IEEE International Symposium on Diagnostics for Electrical Machines, Power Electronics and Drives (IEEE SDEMPED'01), pp. 367-372, Grado, Italy, September 1-3, 2001.

A Coupled Electromagnetic Transformer Model for the Analysis of Winding Inter-Turn Short-Circuits

Luís M. R. Oliveira [1] [2] A. J. Marques Cardoso [1]

[1] Universidade de Coimbra, Departamento de Engenharia Electrotécnica
Pólo II - Pinhal de Marrocos, P – 3030-290 Coimbra, Portugal

[2] Escola Superior de Tecnologia da Universidade do Algarve
Campus da Penha, P – 8000-117 Faro, Portugal

***Abstract* — This paper presents the development and implementation of a coupled electromagnetic transformer model for the simulation of three-phase power and distribution transformers affected by the presence of winding inter-turn short-circuits. Generically, the coupled electromagnetic transformer model is based on the simultaneous consideration of both magnetic and electric equivalent circuits. To incorporate the internal faults in this model a suitable equivalent circuit of the faulty winding is proposed. Both simulation and laboratory tests results are presented in the paper, which demonstrate the adequacy of the proposed model.**

***Index Terms* — Transformers; modelling and simulation; coupled electromagnetic model; winding inter-turn short--circuit faults; Park's Vector Approach.**

I. INTRODUCTION

The sweeping changes that have overtaken the electricity supply industry during the closing decade of the 20th century have created a powerful new commercial climate. Power utilities and supply companies must now compete in increasingly open, de-regulated markets, on an increasingly international scale. To ensure commercial survival in this aggressively competitive environment, it is essential that key items of power generation plants and power transmission and distribution networks not only operate efficiently, but with maximum availability and with the lowest possible cost of ownership over – and frequently beyond – their design life. Power and distribution transformers have formed an essential part of electricity supply networks since the alternating current system was adopted more than a century ago [1]. Therefore it is quite obvious the need for the development of on-line diagnostic techniques, that would aid in transformers maintenance. A survey of the most important methods, actually in use, for condition monitoring and diagnostics of power and distribution transformers, presented in [2], stresses the need for the development of new diagnostic techniques, which can be applied without taking transformers out of service, and which can also provide a fault severity criteria, in particular for determining transformers winding faults.

Preliminary experimental results, presented in [2], concerning the use of the Park's Vector Approach, have demonstrated the effectiveness of this non-invasive technique for diagnosing the occurrence of inter-turn short-circuits in the windings of operating three-phase transformers.

In order to obtain a deeper knowledge in the study of inter-turn short-circuits occurrence, and also to acquire a generalised perspective of this phenomenon, it becomes necessary to develop a digital model for internal fault studies in three-phase power and distribution transformers, which is the scope of this paper.

For this type of studies, an open-structure transformer model is necessary, i.e., a model in which it would be possible to manipulate the windings arrangement. The coupled electromagnetic model [3-6], allowing for the modelling and simulation of the transformer in its natural technology, so that the cause-and-effect relationships can be closely investigated [4], becomes the natural choice for the analysis of transformer internal faults.

II. TRANSFORMER MODEL FOR NORMAL OPERATING CONDITIONS ANALYSIS [3]

The coupled electromagnetic transformer model consists in the combination of both magnetic and electrical equivalent circuits, in order to obtain the flux-current relationships. A typical flux distribution for a three-phase, three-limb, two-winding, core-type transformer is sketched in Fig. 1(a). Taking advantage of the vertical symmetry of the transformer, the magnetic equivalent circuit can be derived, as shown in Fig. 1(b), consisting of magnetomotive forces (*MMF*), f_i, and lumped (linear and non-linear) permeances, P_i. As a first approach, let's consider only the excited windings and neglect the leakage fluxes associated with each winding. In a similar manner to that presented in [3, 6], the flux-*MMF* non-linear relation (ϕ–f) can be expressed as:

$$\begin{bmatrix}\phi_1\\ \phi_2\\ \phi_3\end{bmatrix}=\begin{bmatrix}a_{11} & a_{12} & a_{13}\\ a_{12} & a_{22} & a_{23}\\ a_{13} & a_{23} & a_{33}\end{bmatrix}\cdot\begin{bmatrix}f_1\\ f_2\\ f_3\end{bmatrix}\Rightarrow \boldsymbol{\phi}_i=\boldsymbol{A}\cdot\boldsymbol{f}_i \tag{1}$$

where:

$$a_{11}=\tfrac{1}{2}P_1\left[1-P_1\left(P_{22}P_{33}-P_{23}^2\right)\big/D\right] \tag{2a}$$

$$a_{12}=\tfrac{1}{2}P_1P_2P_{12}P_{33}\big/D \tag{2b}$$

$$a_{13}=-\tfrac{1}{2}P_1P_3P_{12}P_{23}\big/D \tag{2c}$$

$$a_{22}=\tfrac{1}{2}P_2\left[1-\left(P_2P_{11}P_{33}\right)\big/D\right] \tag{2d}$$

$$a_{23}=\tfrac{1}{2}P_2P_3P_{11}P_{23}\big/D \tag{2e}$$

$$a_{33}=\tfrac{1}{2}P_3\left[1-P_3\left(P_{11}\cdot P_{22}-P_{12}^2\right)\big/D\right] \tag{2f}$$

$$D = |\boldsymbol{A}| = P_{11} \cdot P_{22} \cdot P_{33} - P_{11} \cdot P_{23}^2 - P_{33} \cdot P_{12}^2 \quad (2g)$$

and:

$$P_{11} = P_1 + P_4 + P_{01} \quad (3a)$$

$$P_{12} = -P_4 \quad (3b)$$

$$P_{22} = P_2 + P_4 + P_5 + P_{02} \quad (3c)$$

$$P_{23} = -P_5 \quad (3d)$$

$$P_{33} = P_3 + P_5 + P_{03} \quad (3e)$$

Recognising that $f = N_1 i$ and $\lambda = N_1 \phi$, the main linkage fluxes, which do not take into account the leakage fluxes, can be expressed, from (1), as:

$$\boldsymbol{\lambda}_h = N_1^2 \boldsymbol{A} \cdot \boldsymbol{i} \quad (4)$$

The total linkage fluxes can now be computed, introducing the leakage fluxes, as follows:

$$\boldsymbol{\lambda}_t = \boldsymbol{\lambda}_h + \boldsymbol{L}_\sigma \cdot \boldsymbol{i} = \boldsymbol{L} \cdot \boldsymbol{i} \quad (5)$$

being $\boldsymbol{L}_\sigma$ the diagonal leakage inductance matrix. It is assumed that there is an individual leakage inductance associated with each winding, which is determined from the conventional short-circuit test, where the per-unit primary and secondary leakage inductances are equal, $l_{\sigma p} = l_{\sigma s} = l_{cc}/2$ (p.u.).

When the transformer's secondary-side is loaded, there are two *MMF*'s in each limb. It is now necessary to expand (1), as follows:

$$\begin{bmatrix} \phi_1 \\ \phi_2 \\ \phi_3 \end{bmatrix} = \begin{bmatrix} a_{11} & a_{12} & a_{13} \\ a_{12} & a_{22} & a_{23} \\ a_{13} & a_{23} & a_{33} \end{bmatrix} \cdot \begin{bmatrix} N_1 i_1 + N_2 i_4 \\ N_1 i_2 + N_2 i_5 \\ N_1 i_3 + N_2 i_6 \end{bmatrix} \quad (6)$$

which leads to a system of six equations:

$$\boldsymbol{i} = \boldsymbol{\Gamma} \cdot \boldsymbol{\lambda_t} \quad (7)$$

where:

$$\boldsymbol{\Gamma} = \boldsymbol{L}^{-1} = \left[\begin{bmatrix} N_1^2 \cdot \boldsymbol{A} & N_1 \cdot N_2 \cdot \boldsymbol{A} \\ N_1 \cdot N_2 \cdot \boldsymbol{A} & N_2^2 \cdot \boldsymbol{A} \end{bmatrix} + \boldsymbol{L}_\sigma \right]^{-1} \quad (8)$$

The winding connections are established, in the model, from the equivalent electric circuit, which is shown in Fig. 2 for the case of an *Ynyn*0 connection and a balanced resistive load. The equations that describe the terminal conditions at each winding can be expressed as:

$$\frac{d\boldsymbol{\lambda_t}}{dt} = \boldsymbol{v} - \boldsymbol{R} \cdot \boldsymbol{i} \quad (9)$$

where:

$$\boldsymbol{\lambda}_t = \begin{bmatrix} \lambda_{t1} & \lambda_{t2} & \lambda_{t3} & \lambda_{t4} & \lambda_{t5} & \lambda_{t6} \end{bmatrix}^T \quad (10)$$

$$\boldsymbol{v} = \begin{bmatrix} v_{1n} & v_{2n} & v_{3n} & 0 & 0 & 0 \end{bmatrix}^T \quad (11)$$

$$\boldsymbol{i} = \begin{bmatrix} i_1 & i_2 & i_3 & i_4 & i_5 & i_6 \end{bmatrix}^T \quad (12)$$

$$\boldsymbol{R} = \mathrm{diag}\left[R_p \;\; R_p \;\; R_p \;\; (R_s + R_L) \;\; (R_s + R_L) \;\; (R_s + R_L) \right] \quad (13)$$

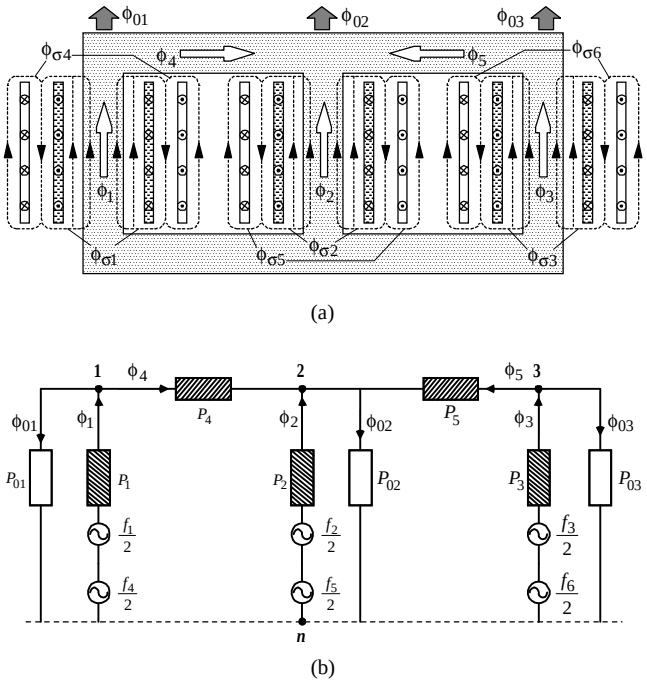

Fig. 1: (a) Flux distribution in a three-phase, three-limb, two-winding, core-type transformer, assuming a slightly greater magnetomotive force in the inner windings; (b) equivalent magnetic circuit.

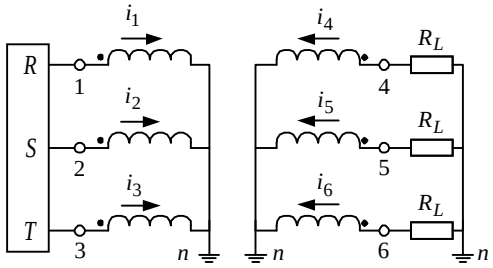

Fig. 2: Simplified equivalent electric circuit for the case of an *Ynyn*0 connection and a balanced resistive load.

being R_p and R_s the primary and secondary winding resistances, respectively.

In order to maintain a trade off between complexity and accuracy, an approximation was made to include the excitation losses, by connecting three linear resistance branches across the terminals of the excited windings.

The influence of the no-load losses conductances, G_{fe}, can now be introduced in (7):

$$\boldsymbol{i} = \boldsymbol{\Gamma} \cdot \boldsymbol{\lambda_t} + \boldsymbol{G_{fe}} \cdot \boldsymbol{v} \quad (14)$$

being $\boldsymbol{G_{fe}}$ a 6×6 matrix, where only the first 3×3 diagonal sub-matrix has non-zero values.

The electromagnetic coupled transformer model is thus based on the combination of (9) and (14), which takes into account the asymmetry and saturation effects of the core. The development, implementation and validation of the transformer non-linear model, for normal operating conditions analysis, was presented in a previous paper [3], where a good agreement was achieved for both simulation and experimental test results.

III. MODELLING WINDING INTER-TURN SHORT-CIRCUIT FAULTS

To incorporate the internal faults in the aforementioned model, the faulty winding is divided into two parts: the healthy part (N_a turns) and the faulty part (N_b turns), as shown in Fig. 3, for the case of a fault in the primary winding (phase *R*), localised in the bottom part of the coil.

The primary-side short-circuited turns will act as an auto-transformer load on the primary winding [7], as shown in Fig. 3, where R_{sh} represents the fault impedance. The resultant magnetic equivalent circuit is shown in Fig. 4, leading to three magnetomotive forces in the limb of the faulty phase. From the equivalent magnetic circuit, the ϕ–f relationship becomes:

$$\begin{bmatrix}\phi_1\\ \phi_2\\ \phi_3\end{bmatrix}=\begin{bmatrix}a_{11} & a_{12} & a_{13}\\ a_{12} & a_{22} & a_{23}\\ a_{13} & a_{23} & a_{33}\end{bmatrix}\cdot\begin{bmatrix}N_a\, i_1+N_a\, i_b+N_2\, i_4\\ N_1\, i_2+N_2\, i_5\\ N_1\, i_3+N_2\, i_6\end{bmatrix} \quad (15)$$

The resultant main linkage fluxes are:

$$\begin{cases}\lambda_{h1}=N_1\phi_1\\ \lambda_{h2}=N_1\phi_2\\ \lambda_{h3}=N_1\phi_3\\ \lambda_{hb}=N_b\phi_1\end{cases}\qquad\begin{cases}\lambda_{h4}=N_2\phi_1\\ \lambda_{h5}=N_2\phi_2\\ \lambda_{h6}=N_2\phi_3\end{cases} \quad (16)$$

from which the relation expressed by (7) can be computed, using:

$$\boldsymbol{\lambda}_t=\begin{bmatrix}\lambda_{t1} & \lambda_{t2} & \lambda_{t3} & \lambda_{tb} & \lambda_{t4} & \lambda_{t5} & \lambda_{t6}\end{bmatrix}^T \quad (17)$$

$$\boldsymbol{i}=\begin{bmatrix}i_1 & i_2 & i_3 & i_b & i_4 & i_5 & i_6\end{bmatrix}^T \quad (18)$$

$$\boldsymbol{\Gamma}=\boldsymbol{L}^{-1}=\begin{bmatrix}\boldsymbol{L_{AA}} & \boldsymbol{L_{AB}}\\ \boldsymbol{L_{BA}} & \boldsymbol{L_{BB}}\end{bmatrix}^{-1} \quad (19)$$

where:

$$\boldsymbol{L_{AA}}=\begin{bmatrix}N_1N_aa_{11}+L_{\sigma a} & N_1^2a_{12} & N_1^2a_{13} & N_1N_ba_{11}+L_{\sigma b}\\ N_1N_aa_{12} & N_1^2a_{22}+L_{\sigma p} & N_1^2a_{23} & N_1N_ba_{12}\\ N_1N_aa_{13} & N_1^2a_{23} & N_1^2a_{33}+L_{\sigma p} & N_1N_ba_{13}\\ N_bN_aa_{11} & N_bN_1a_{12} & N_bN_1a_{13} & N_b^2a_{11}+L_{\sigma b}\end{bmatrix} \quad (20)$$

$$\boldsymbol{L_{AB}}=\begin{bmatrix}N_1N_2a_{11} & N_1N_2a_{12} & N_1N_2a_{13}\\ N_1N_2a_{12} & N_1N_2a_{22} & N_1N_2a_{23}\\ N_1N_2a_{13} & N_1N_2a_{23} & N_1N_2a_{33}\\ N_bN_2a_{11} & N_bN_2a_{12} & N_bN_2a_{13}\end{bmatrix} \quad (21)$$

$$\boldsymbol{L_{BA}}=\begin{bmatrix}N_2N_aa_{11} & N_2N_1a_{12} & N_2N_1a_{13} & N_2N_ba_{11}\\ N_2N_aa_{12} & N_2N_1a_{22} & N_2N_1a_{23} & N_2N_ba_{12}\\ N_2N_aa_{13} & N_2N_1a_{23} & N_2N_1a_{33} & N_2N_ba_{13}\end{bmatrix} \quad (22)$$

$$\boldsymbol{L_{BB}}=\begin{bmatrix}N_2^2a_{11}+L_{\sigma s} & N_2^2a_{12} & N_2^2a_{13}\\ N_2^2a_{12} & N_2^2a_{22}+L_{\sigma s} & N_2^2a_{23}\\ N_2^2a_{13} & N_2^2a_{23} & N_2^2a_{33}+L_{\sigma s}\end{bmatrix} \quad (23)$$

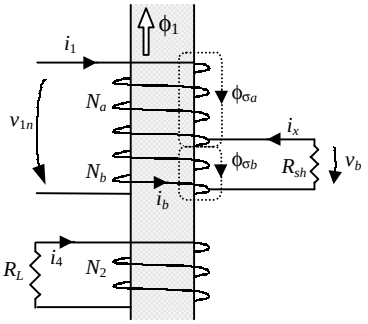

Fig. 3: Equivalent circuit for a fault localised in the bottom part of the primary winding (phase *R*).

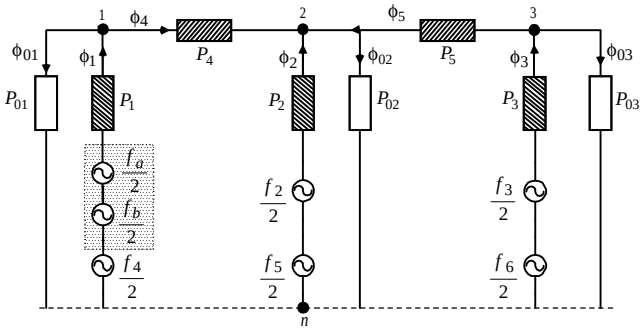

Fig. 4: Equivalent magnetic circuit for the case of a primary-side faulty winding (phase *R*).

being $L_{\sigma a}$ and $L_{\sigma b}$ the leakage inductances associated with the subwindings *a* and *b*, respectively.

For the same type of fault, the corresponding electric equivalent circuit is shown in Fig. 5. The generic differential equation (9) still holds, but now with the fluxes vector of (17), the currents vector of (18) and:

$$\boldsymbol{v}=\begin{bmatrix}v_{1n} & v_{2n} & v_{3n} & 0 & 0 & 0 & 0\end{bmatrix}^T \quad (24)$$

$$\boldsymbol{R}=\begin{bmatrix}R_a & 0 & 0 & R_b & 0 & 0 & 0\\ 0 & R_p & 0 & 0 & 0 & 0 & 0\\ 0 & 0 & R_p & 0 & 0 & 0 & 0\\ -R_{sh} & 0 & 0 & R_{sh}+R_b & 0 & 0 & 0\\ 0 & 0 & 0 & 0 & R_S+R_L & 0 & 0\\ 0 & 0 & 0 & 0 & 0 & R_S+R_L & 0\\ 0 & 0 & 0 & 0 & 0 & 0 & R_S+R_L\end{bmatrix} \quad (25)$$

where R_a and R_b are the resistances of the subwindings *a* and *b*, respectively.

With this approach, the only additional data required for modelling winding inter-turn short-circuit faults, as compared to the healthy transformer model, are the leakage inductances and the resistances of the subwindings *a* and *b*.

Several short-circuit tests and analytical studies were conducted to determine $L_{\sigma a}$ and $L_{\sigma b}$. It seems, however, that a good approximation is obtained, for a generic *k* subwinding, by using:

$$L_{\sigma k}=\frac{N_k}{N_1}L_{\sigma p} \quad (26)$$

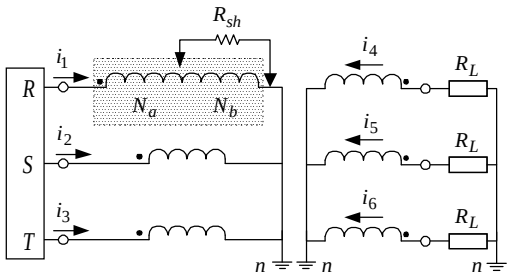

Fig. 5: Equivalent electric circuit for the case of a primary-side faulty winding (phase *R*).

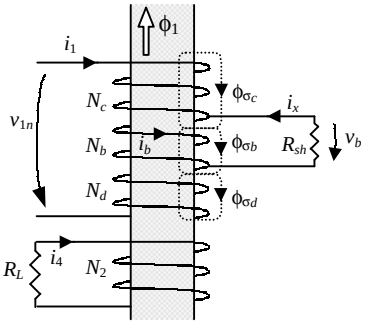

Fig. 6: Equivalent circuit of a fault in the middle part of the primary winding (phase *R*).

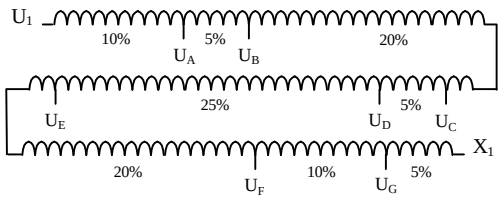

Fig. 7: Location of the tappings for transformer primary winding (phase *R*).

Additionally, the leakage inductances do not change significantly with the fault position along the affected winding.

The subwindings resistances are also determined by a linear relationship based on the corresponding turns ratio:

$$R_k = \frac{N_k}{N_1} R_p \tag{27}$$

If the fault is localised in the upper part of the coil, the same methodology applies.

For a fault location in the middle part of the primary winding, although two healthy subwindings (N_c and N_d turns) and one faulty subwinding (N_b turns) have to be considered (Fig. 6), the same methodology can also be applied, assuming $N_a = N_c + N_d$. With the approximations of (26) and (27), which results in $L_{\sigma a} = L_{\sigma c} + L_{\sigma d}$ and in $R_a = R_c + R_d$, respectively, the relations (17) to (25) remain valid.

IV. MODEL VALIDATION

For the model validation, a three-phase, three-limb transformer, of 6 kVA, 220/127 V, was used. The transformer has two windings per phase on the primary and on the secondary side, having, one of each, been modified by the addition of a number of tappings connected to the coils, for each of the three phases, allowing for the introduction of different percentages of shorted turns at several locations in the winding, as shown in Fig. 7 for the phase *R* of the transformer primary winding [2].

A shorting resistor was connected at the terminals of the faulty subwinding, whose value was chosen so as to create an effect strong enough to be easily visualised, but simultaneously big enough to limit the short-circuit current and thus protecting the test transformer from complete failure when the short is introduced.

Both harmonic magnitudes and harmonic phase angles of the supply voltages were taken into account in the conducted simulation study.

For the case of the *Ynyn*0 connection, a balanced resistor load and 10% of shorted turns in the phase *R* of the transformer primary winding, both experimental and simulated primary-side currents waveforms are shown in Fig 8(a) and 8(b), respectively, which are in relatively good agreement.

The occurrence of primary-side inter-turn short-circuits leads to an increment in the magnitude of the current in the affected winding, as compared to an healthy condition, which results in an unbalanced system of primary currents. For this reason, the magnitude of the primary neutral current ($i_{n1}=i_1+i_2+i_3$) is also affected.

In the presence of the primary winding inter-turn short--circuits, the secondary side currents do not present any relevant change as compared to the transformer's healthy operation, remaining an approximately balanced three--phase system (Fig. 9).

For the same aforementioned conditions, the experimental and simulated fault related currents waveforms are shown in Fig. 10(a) and 10(b). The faulty subwinding current, i_b, is approximately in phase opposition with i_1 (*Lenz* law). The current in the short-circuit auxiliary resistor, i_x, has a higher magnitude than i_b, since $i_x = i_b - i_1$.

For the same load conditions and transformer winding connections mentioned above, Fig. 11 presents the experimental primary side current Park's Vector patterns, for several percentages of shorted turns in the primary windings and for different faulty phases. The primary side current Park's Vector pattern, corresponding to the healthy operation, differs slightly from the circular locus expected for ideal conditions, due to, among others, the supply voltage harmonic content and the minor reluctance seen from the central limb, with respect to the lateral limbs [2].

The occurrence of primary-side inter-turn short-circuits manifests itself in the deformation of the supply current Park's Vector pattern corresponding to a healthy condition, leading to an elliptic representation, whose ellipticity increases with the severity of the fault and whose major axis orientation is associated to the faulty phase [2].

The simulated primary-side current Park's Vector patterns are presented in Fig. 12, which are in close agreement with the experimental results of Fig. 11.

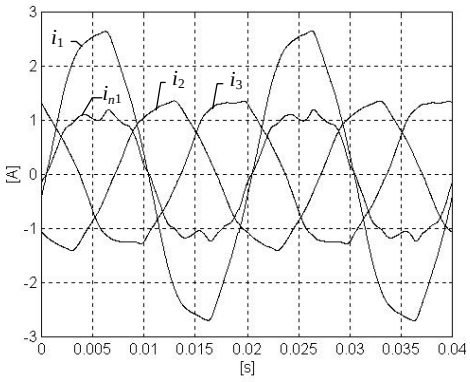

(a)

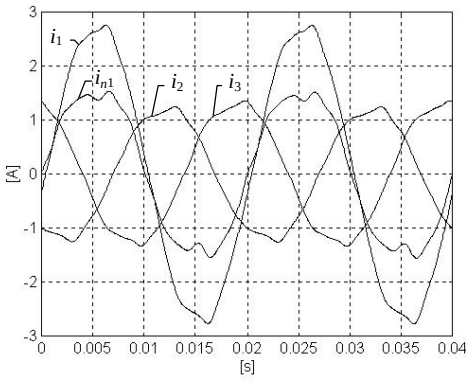

(b)

Fig. 8: Primary-side currents waveforms for the case of an *Ynyn*0 connection, a pure resistive balanced load and 10% of shorted turns in the primary winding (phase *R*): (a) experimental; (b) simulated.

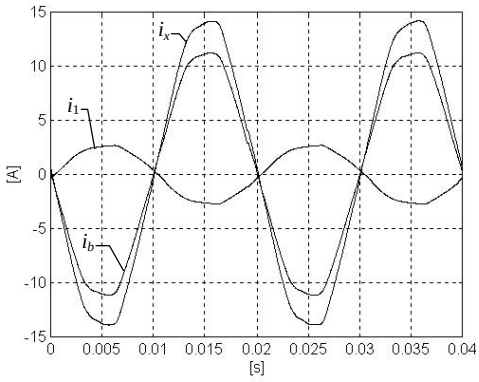

(a)

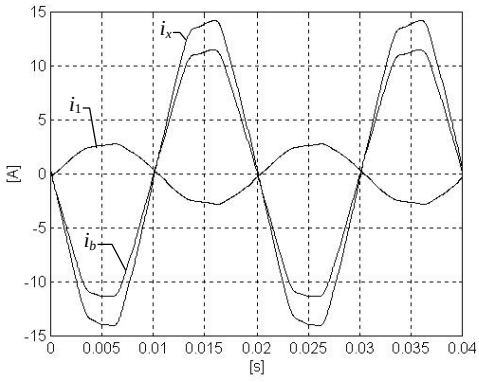

(b)

Fig. 10: Fault related currents waveforms for the case of an *Ynyn*0 connection, a pure resistive balanced load and 10% of shorted turns in the primary winding (phase *R*): (a) experimental; (b) simulated.

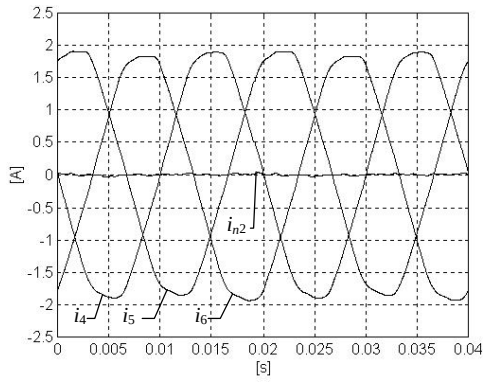

(a)

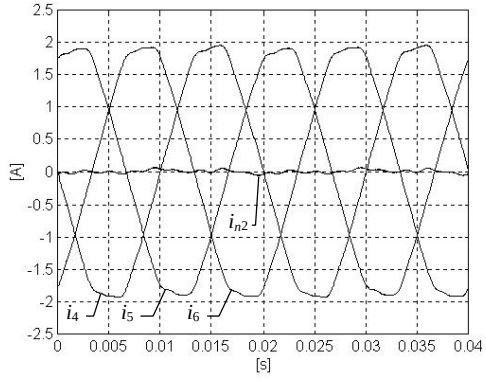

(b)

Fig. 9: Secondary-side currents waveforms for the case of an *Ynyn*0 connection, a pure resistive balanced load and 10% of shorted turns in the primary winding (phase *R*): (a) experimental; (b) simulated.

V. CONCLUSIONS

This paper describes the development and implementation of a coupled electromagnetic transformer model for the analysis of winding inter-turn short-circuits. The model is based on the combination of both magnetic and electric lumped-parameters equivalents circuits, which allows the modelling and simulation of the transformer in its natural technology.

The faults are introduced in the model by dividing the affected winding in two parts, which represents the healthy subwinding and the faulty subwinding. With this approach, the primary-side short-circuited turns will act as an auto-transformer load on the primary winding. The open structure of the coupled electromagnetic model is perfectly compatible with the fault auto-transformer equivalent circuit, which allows to study these phenomena from a physical perspective. Both simulation and experimental tests results demonstrate the adequacy of the model, under healthy and faulty operating conditions.

With the supply current Park's Vector pattern, it is possible to diagnose primary winding inter-turn short--circuits faults. The on-line diagnosis is based on identifying the appearance of an elliptic pattern, corresponding to the transformer supply current Park's Vector representation, whose ellipticity increases with the severity of the fault and whose major axis orientation is associated to the faulty phase.

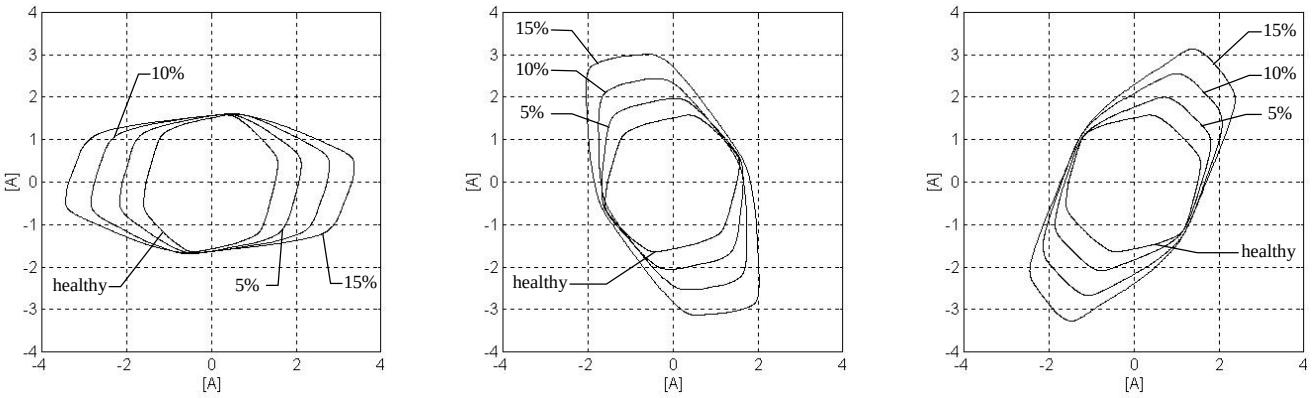

(a) (b) (c)

Fig. 11: Experimental primary-side current Park's Vector patterns for the case of an *Ynyn*0 connection and a balanced resistive load, with several percentages of shorted turns in the primary windings and for different faulty phases: (a) phase *R*; (b) phase *S*; (c) phase *T*.

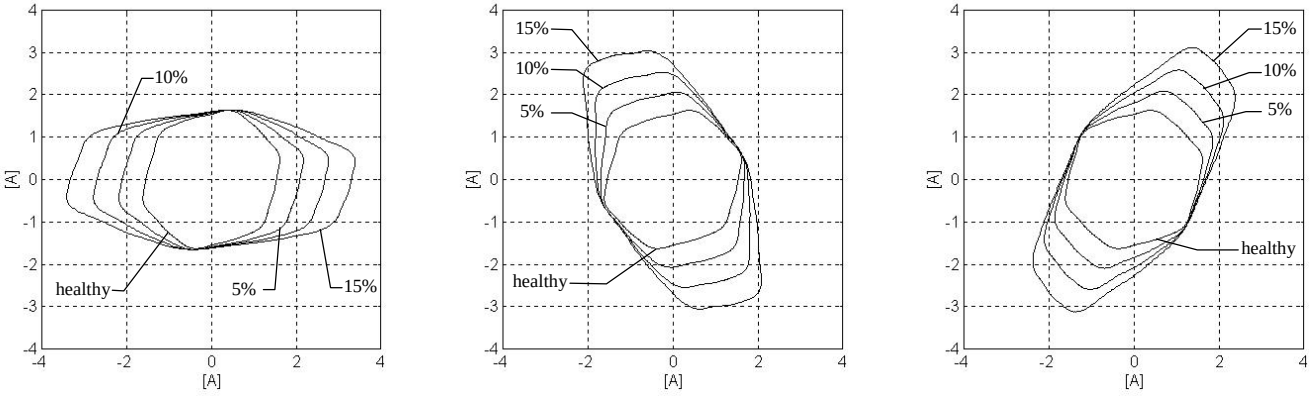

(a) (b) (c)

Fig. 12: Simulated primary-side current Park's Vector patterns for the case of an *Ynyn*0 connection and a balanced resistive load, with several percentages of shorted turns in the primary windings and for different faulty phases: (a) phase *R*; (b) phase *S*; (c) phase *T*.

Further work is currently in progress, concerning the modelling and simulation of the behaviour of three-phase transformers, under the influence of the simultaneous occurrence of winding faults, unbalanced supply voltages, unbalanced loads, or even the surrounding presence of power electronics equipment. Additionally, a more accurate method to determine the subwindings leakage inductances will be also investigated.

ACKNOWLEDGEMENT

The authors wish to acknowledge the financial support of the Portuguese Foundation for Science and Technology, under Project Number PRAXIS/P/EEI/14151/1998.

REFERENCES

[1] Ashmore, C. "Transforming technology" *International Power Generation*, Vol. 22, Nº 3, pp. 25-26, March 1999.

[2] Cardoso, A. J. M. ; Oliveira, L. M. R. "Condition monitoring and diagnostics of power transformers" *International Journal of COMADEM*, Vol. 2, Nº 3, pp. 5-11, July 1999.

[3] Oliveira, L. M. R.; Cardoso, A. J. M. "Three-Phase, three-limb, steady-state transformer model: The case of a *Ynzn* connection" Proceedings of the IASTED International Conference, "Power and Energy Systems", Marbella, Spain, pp. 491-472, September 2000.

[4] Yacamini, R.; Bronzeado, H. "Transformer inrush calculations using a coupled electromagnetic model" *IEE Proc. Sci. Meas. Technol.*, Vol. 141, Nº 6, pp. 491-498, November 1994.

[5] Elleuch, M.; Poloujadoff, M. "A contribution to the modelling of three phase transformers using reluctances" *IEEE Trans. on Magnetics*, Vol. 32, Nº. 2, pp. 335-343, March 1996.

[6] Chen, X. S.; Neudorfer, P. "Digital model for transient studies of a three-phase five-legged transformer" *IEE Proc. Pt. C*, Vol. 139, Nº 4, pp. 351-359, July 1992.

[7] Stigant, S. A.; Franklin, A. C., *The J & P Transformer Book*, 10th Edition, London, Newnes-Butterworths, 1973.